buildings

MDPI

*Article*

# Study on Mechanical Properties and Microstructure of Basalt Fiber Reactive Powder Concrete

**Mo Liu [1], Wenting Dai [1,*], Chunling Zhong [2] and Xue Yang [1]**

[1] College of Construction Engineering, Jilin University, Changchun 130026, China
[2] School of Economics and Management, Jilin Jianzhu University, Changchun 130000, China
* Correspondence: daiwt@jlu.edu.cn

**Abstract:** In order to promote the wide application of reactive powder concrete (RPC) in practical engineering. In this paper, RPC was prepared using conventional and economical natural river sand instead of quartz sand and economical and environmentally friendly basalt fiber (BF) instead of steel fiber, and the macroscopic properties of basalt fiber reactive powder concrete (BFRPC) with different fiber content, such as flowability, failure mode, compressive strength and splitting tensile strength were studied, and the strength calculation formula of BFRPC was established based on the mechanical property results. The microscopic morphology and structure of BFRPC were characterized by scanning electron microscope (SEM) and Image Pro Plus (IPP) image processing software. The results show that BF has a small effect on the compressive strength of RPC, while it has a significant increase on the splitting tensile strength. When BF content is at 2 kg/m$^3$, the 28-day compressive strength reaches 95.2 MPa and splitting tensile strength reaches 7.78 MPa. Compared with the RPC with BF of 0 kg/m$^3$, the BFRPC shows an improvement in its 28-day compressive strength by 25.70% and an increase in its splitting tensile strength by 83.92%. According to the microscopic analysis, reasonable fiber content can optimize the internal microstructure of BFRPC, but excessive BF content will produce agglomeration and overlap, resulting in strength loss. Based on the gray correlation analysis method, it was concluded that the particle area ratio and pore fraction dimension were the most correlated with the mechanical properties of BFRPC. In addition, the feasibility and applicability of the BFRPC strength calculation formula were summarized. This research results of this paper provides a valuable reference for the further research and promotion of BFRPC.

**Keywords:** basalt fiber; reactive powder concrete; compressive strength; splitting tensile strength; microstructure



**Citation:** Liu, M.; Dai, W.; Zhong, C.; Yang, X. Study on Mechanical Properties and Microstructure of Basalt Fiber Reactive Powder Concrete. *Buildings* **2022**, *12*, 1734. https://doi.org/10.3390/buildings12101734

Academic Editors: Lei Wang and Shengwen Tang

Received: 11 September 2022
Accepted: 9 October 2022
Published: 19 October 2022



## 1. Introduction

With the emergence of super high-rise, long-span, lightweight structures, the requirements for concrete are constantly increasing and have driven the development of concrete with ultrahigh strength, high toughness, and high reliability. As a new type of building structure material, reactive powder concrete (RPC) can meet and adapt to the development of current building structure towards high strength and high durability [1,2]. It lacks the coarse aggregates and instead contains quartz sand, silica fume, and fly ash to reach maximum filling density inside RPC. Through thermal curing, the reaction between components of the material is accelerated, and the bond strength of the interface is improved. In addition, fine steel fiber is incorporated to improve toughness and ductility [3]. Therefore, RPC has great application prospects in construction engineering.

Quartz sand contains a high content of silicon, which accelerates the ash reaction and improves the filling effect at the interface between aggregates [4,5]. It can also enhance the compactness of RPC matrix and reduce internal porosity. Silica sand contributes negatively to RPC under certain circumstances. However, in some cases, quartz sand reduces RPC strength by filling the internal voids and reducing the pozzolanic reaction between silica

powder and cement [6]. Although quartz sand has certain advantages in RPC, the uneven distribution of quartz sand resources requires high production and transportation costs and, consequently, increases the production cost of RPC. High-quality natural river sand is similar to quartz sand in chemical composition, grain shape, and particle size and has abundant sources and low prices. Mao et al. showed that when natural river sand was used to substitute crushed stone quartz for RPC preparation, the 28-day compressive strength was reduced by 9–14%. Considering the cost and mechanical properties, the use of natural river sand instead of gravel as fine aggregate in RPC has high application value [7]. This raw material provides good economic benefits and has engineering significance.

Curing condition is the key factor to prepare RPC with excellent performance [5,8]. Thermal curing contributes to the early strength development of RPC, which makes the compressive strength of RPC reach more than 100 Mpa in a short time [3]. Compared with RPC without fiber, the compressive strength can be increased by 10–15% using heat curing treatment and adding fine steel fiber [9]. The preset time and pressure of autoclaved curing are the key factors affecting RPC performance [10]. In the presence of simultaneous heat and pressure, the internal pores can be filled rapidly. Therefore, the RPC strength can be significantly increased in a short period of time [3,11]. However, excessive preset pressure will cause the aggregate to expand and generate microcracks, thus reducing the strength [12,13]. Although thermal curing and autoclaved curing contribute to the performance of RPC, thermal curing requires a large number of equipment and sites and increases the difficulty of on-site construction, which limits its application in on-site construction. Therefore, RPC preparation under conventional curing conditions must be studied to promote its wide application in practical engineering.

Incorporating fiber in concrete usually has excellent properties, effectively improving the crack resistance, tensile strength, and load-bearing capacity of concrete [14,15]. Steel fiber can limit the crack development of RPC matrix, thus improving the strength and crack resistance of RPC [16–20]. The size and content of different steel fiber can affect the performance of RPC to a certain extent [21–23]. The results show that, compared with the compressive strength, the steel fiber increases the splitting tensile strength and flexural strength of RPC more obviously [24–26]. Therefore, the incorporation of steel fiber into RPC has a broad application prospect in practical engineering. However, the production cost of steel fiber is high, and its corrosion resistance is poor, especially in harsh environments, such as saline–alkali land and marine environment. This characteristic has a serious effect on the service life and bearing life of the structure. Ultrafine stainless steel wire and carbon fiber have also been used to prepare RPC. Ultrafine stainless steel wire has a micron-scale diameter and a high specific surface area, allowing it to form a widely distributed grid in the matrix to improve the weak interface area and the RPC matrix. The compactness of RPC can significantly improve its toughness by transmitting the crack intermittent stress and inhibiting the initiation and propagation of cracks [27,28]. RPC with appropriate carbon fiber content has good mechanical properties and self-sensing properties [29]. Moreover, the contribution of carbon fiber to the mechanical properties of RPC is lower than that of steel fiber [30,31]. However, ultrafine stainless steel wire and carbon fiber are expensive, and thus increase the production cost. Therefore, the preparation of economic and reasonable RPC is an inevitable trend.

With people's close attention to environmental protection, energy saving, and emission reduction, the use of green environmental protection materials has become the development direction and inevitable trend of the construction industry. Basalt fiber (BF) is a new economic and green fiber made of natural basalt rock by melting and stretching [32]. It has excellent mechanical properties and corrosion resistance and has been widely used in many fields. BF can effectively fuse with cement-based matrix, making the inner part of the matrix more compact [33], and it can resist the generation and expansion of cracks, effectively improving the mechanical properties, crack resistance, and ductility of cement materials [33–39]. The modulus of the elasticity of BF is much higher than that of chemical fiber, such as polypropylene fiber and polyvinyl alcohol fiber. Different BF lengths

have varying effects on concrete strength. Short-sized BF (12 mm) contribute more to the compressive strength of concrete than long-sized BF (25 mm, 37 mm, 50 mm) [40]. Compared with steel fiber, BF has good corrosion resistance and cheap price. In addition, BF is superior to polypropylene fiber in the contribution of concrete compressive strength [41]. Ahmet B showed that BF concrete has better crack resistance and ductility than glass fiber concrete [32] and is cheaper than carbon fiber concrete. In addition, BF can also improve the durability of concrete. Ding [42] showed that BF can effectively improve the anti-carbonation properties of recycled concrete, but the anti-carbonation properties can be reduced by incorporating too much. Lu [43] showed that the addition of BF could inhibit high temperature carbonation of concrete, reduce the thickness of the burnt layer, and significantly improve the chloride ion penetration resistance of concrete. Meanwhile, with the increase in erosion age, the concentration increased rapidly in the initial stage, and the pore structure was optimized in the later stage with the continuous hydration process, and the gradual increase rate of erosion concentration decreased [44,45]. Wang [46] showed that the appropriate amount of BF can improve the resistance of concrete to sulfate attack. Ren [47] showed that erosion became more pronounced with increasing sulfate concentration and time. Fan [48] showed that BF can significantly improve the freeze–thaw resistance of concrete. After 100 freeze–thaw cycles, the dynamic elastic modulus of BF concrete was 1.47 times higher than that of ordinary concrete, and the mass loss was 0.64 times higher than that of ordinary concrete. Therefore, BF has a wide application prospect in the field of construction and can become a suitable substitute for steel fiber, glass fiber, polypropylene fiber, and carbon fiber [49,50]. Researchers have prepared common concrete mixed with BF and obtained a high performance. However, the study of BFRPC is still in the exploratory stage. Therefore, the present work investigated the macro mechanical properties and microstructure of BFRPC to lay the foundation for its practical engineering application.

RPC research still has some deficiencies. The selection of economical and reasonable materials and the preparation of RPC by conventional maintenance methods are the keys to solving the difficulty in popularizing and applying this material in practical engineering. In this paper, BFRPC was prepared by using economical ordinary conventional materials and standard curing methods, and the working performance and macroscopic mechanical properties of RPC with different dosage of BF were studied, so as to find the optimal dosage of BFRPC. The micromorphology of BFRPC was characterized and analyzed by scanning electron microscope (SEM), and the microstructure was quantitatively analyzed by Image Pro Plus (IPP) software. The relationship between macroscopic mechanical properties and microscopic mechanism of BFRPC was clarified. On this basis, a scientific and reasonable mechanical property calculation formula of BFRPC is established, which provides valuable reference basis for the wide application of BFRPC.

## 2. Materials and Methods

### *2.1. Materials*

The test uses grade 52.5 cement produced by Yatai Cement Factory, which conforms to the general Portland Cement Inspection Standard (GB175-2007) [51]. Grade I fly ash was obtained from Xiao Haibao Superfine Bead Technology Development Co., Henan, China. Silica fume was obtained from Boken Silicon Material Co., Shandong, China. All of these were in accordance with the technical specifications of the Application of Mineral Admixtures (GB/T51003/2014) [52]. The superplasticizer was obtained from Hongxia Polymer Materials Co., Qingdao, China. Fine aggregate uses natural river sand, and the gradation curve is obtained according to sand particle gradation screening test, as shown in Figure 1. BF of 12 mm length produced by Chenqi Chemical Technology Co., Shanghai, China is selected as the fiber. The basic parameters of BF are shown in Table 1, and a picture is shown in Figure 2.

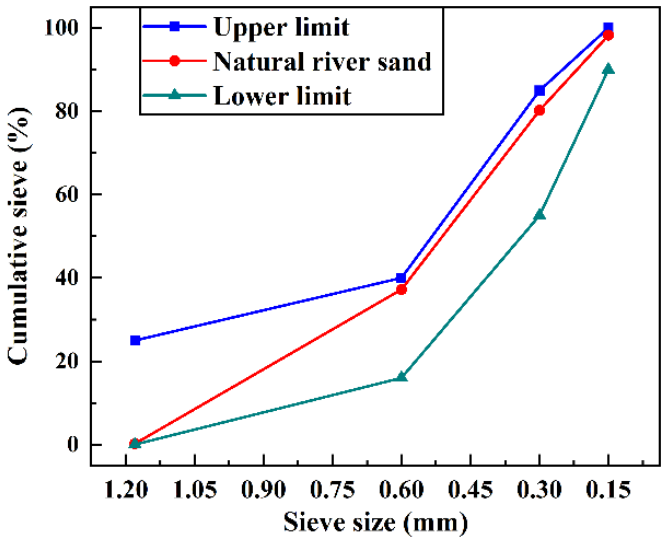


**Figure 1.** Gradation curve of fine aggregates used in the study.

**Table 1.** Basic parameters of basalt fiber.

| Length (mm) | Diameter (μm) | Aspect Ratio | Density (g/cm$^3$) | Elastic Modulus (GPa) | Tensile Strength (MPa) | Elongation at Break (%) |
|---|---|---|---|---|---|---|
| 12 | 17.4 | 689 | 2.7 | 90–110 | 2000 | 1.5–3.2 |


**Figure 2.** Basalt fiber.

### *2.2. Sample Preparation*

On the basis of the optimal mix ratio of RPC matrix obtained in the previous experimental study, 0, 1, 2, 3, and 4 kg/m$^3$ BF were added to prepare BFRPC. The RPC fit ratio and sample number of different BF content are shown in Table 2. An amount of 1 kg of BF is RMB 35, which increases the cost of BFRPC by RMB 35/m$^3$ compared to BF0.

The dispersion uniformity of BF has an important influence on the performance of BFRPC. Therefore, if the fiber can be uniformly dispersed, the properties of the specimens can be effectively improved. It is shown that the friction between sand particles can make the fiber uniformly dispersed [53]. In order to disperse BF more uniformly, most previous studies have used pre-mixing of BF with fine aggregates for dispersion [54–56].

**Table 2.** Mix proportions of BFRPC.

| No. | Water/Binder Ratio | Cement ($kg/m^3$) | Fly Ash ($kg/m^3$) | Silica Fume ($kg/m^3$) | Sand/Binder Ratio | BF Content (BF Volume Fraction) |
|---|---|---|---|---|---|---|
| BF0 | 0.2 | 750 | 200 | 100 | 1.3 | 0 $kg/m^3$ (0%) |
| BF1 | | | | | | 1 $kg/m^3$ (0.037%) |
| BF2 | | | | | | 2 $kg/m^3$ (0.074%) |
| BF3 | | | | | | 3 $kg/m^3$ (0.111%) |
| BF4 | | | | | | 4 $kg/m^3$ (0.148%) |

The process of sample preparation is shown in Figure 3. (i) BF and natural river sand were mixed and stirred for 120 s so that the BF can be dispersed evenly; (ii) cement, fly ash, and silica fume were then added, and the mixture was stirred for 120 s; (iii) 80% mixture of water reducer and water was added, and the mixture was continuously stirred for 240 s; (iv) the remaining mixture of water reducer and water was added, and the mixture was stirred for 120 s; (v) after stirring and molding, the mixture was transferred to the test mold placed on a vibrating table to vibrate the mixture and make it fully dense; (vi) after forming, the specimens were demolded and then cured to 7 and 28 days under standard curing conditions.

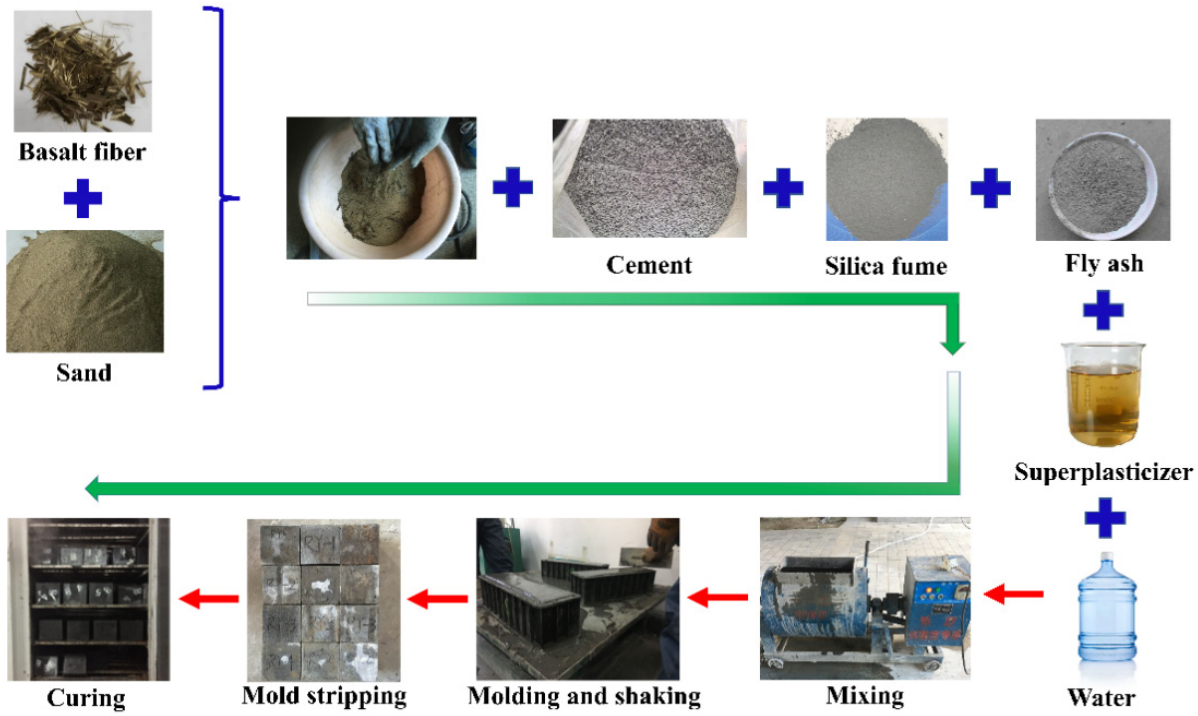


**Figure 3.** Sample preparation process.

### *2.3. Test Methods*

#### 2.3.1. Flowability

Fluidity was tested according to GBT50080-2016 [57]. Slump test is performed by using slump bucket. The slump bucket shall comply with the provisions of JG/T 248-2009 [58].

The mixture was evenly divided into three layers into the slump barrel, the height of each layer of mixture is about 100 mm. In each layer after loading uniform vibration for 25 times, the top layer was tamped to remove the feeding funnel and wiped along the barrel mouth to obtain a flat, vertical, and smooth lift slump barrel. When sample stops slumping, the cylinder height and backward height difference between high mixture was measured as the BFRPC slump value. The expansion degree of the extended mixture was measured with a steel ruler.

#### 2.3.2. Mechanical Properties

The mechanical properties include compressive strength and splitting tensile strength. Test specimens with size of 100 mm × 100 mm × 100 mm were prepared according to Reactive Powder Concrete (GB/T31387-2015) [59]. Three specimens were prepared for each group, and the arithmetic average of the test values of the three specimens was taken as the final test value. The compressive test loading rate was maintained between 1.2 and 1.4 MPa/s, and the loading rate of the splitting tensile strength test was maintained between 0.08 and 0.1 MPa/s.

#### 2.3.3. Microstructure

The combination of stereo optical microscope and digital image processing is considered to be an effective method for the characterization of microstructure and has been widely used in studying the microstructure of materials [60–62].

SEM samples were selected as the damaged specimens closest to the arithmetic mean value in the compressive strength test, and the sample size was about 10 mm. The sample treatment procedures were as follows: (i) sanding the sample with sandpaper to make the surface smooth and smooth, (ii) vacuum-drying the sample, (iii) gold-plating the surface of the sample, and (iv) observing and capturing images using an environmental scanning electron microscope (XL-30).

IPP has powerful filters and contrast adjustment functions that help enhance the image to obtain accurate data results [60–62]. The process of microstructure parameter extraction is as follows. (1) The histeq function of MATLAB is used to process the histogram equalization of the image to make the microstructure clearer and improve the accuracy of data extraction. (2) Using medfilt2 function to carry out median filtering processing on the image. (3) Using fspecial function and Filter2 function to sharpen the image. (4) Image binarization is performed by combining graythresh function and im2bw function. (5) IPP is used to extract pore microscopic parameters from binarized images. (6) The bwdist function and watershed function were used to process the binarized image, and IPP was used to extract particle microscopic parameters from the binarized image after processing.

## 3. Results

### *3.1. Macroscopic Performance Analysis of BFRPC*

The test results of slump, extension, and mechanical properties of BFRPC are shown in Table 3.

**Table 3.** Test results of slump, extension, and mechanical properties of BFRPC.

| No. | Slump (mm) | Extension (mm) | Compressive Strength (MPa) | | Splitting Tensile Strength (MPa) | |
|---|---|---|---|---|---|---|
| | | | 7 Days | 28 Days | 7 Days | 28 Days |
| BF0 | 265 | 350 | 68.90 | 75.77 | 3.49 | 4.23 |
| BF1 | 245 | 315 | 71.93 | 87.82 | 4.97 | 5.48 |
| BF2 | 235 | 300 | 73.61 | 95.24 | 6.08 | 7.78 |
| BF3 | 230 | 290 | 67.49 | 88.00 | 5.24 | 6.76 |
| BF4 | 225 | 280 | 65.78 | 80.61 | 4.75 | 4.39 |

#### 3.1.1. Analysis of Slump and Extension

The slump test is shown in Figure 4. The test results of slump and extension of BFRPC is shown in Figure 5. The incorporation of BFs has a certain influence on the flowability of BFRPC. With the increase in the content of BF, slump, and extension gradually decreased because BF has hydrophilic effect, disperses into a large number of extremely fine flocculent fiber in the mixture, and absorbs part of the free water. BF surface is rough, and its friction coefficient is high. With the increase in the amount added, BF easily coalesced during mixing and absorbed a large amount of cement slurry to wrap. Therefore, the fluidity of BFRPC was weakened. As other studies have shown [63,64], concrete slump decreases

with the increase in BF volume fraction. However, the target slump can be achieved by adding an appropriate amount of superplasticizer.

**Figure 4.** Slump test.

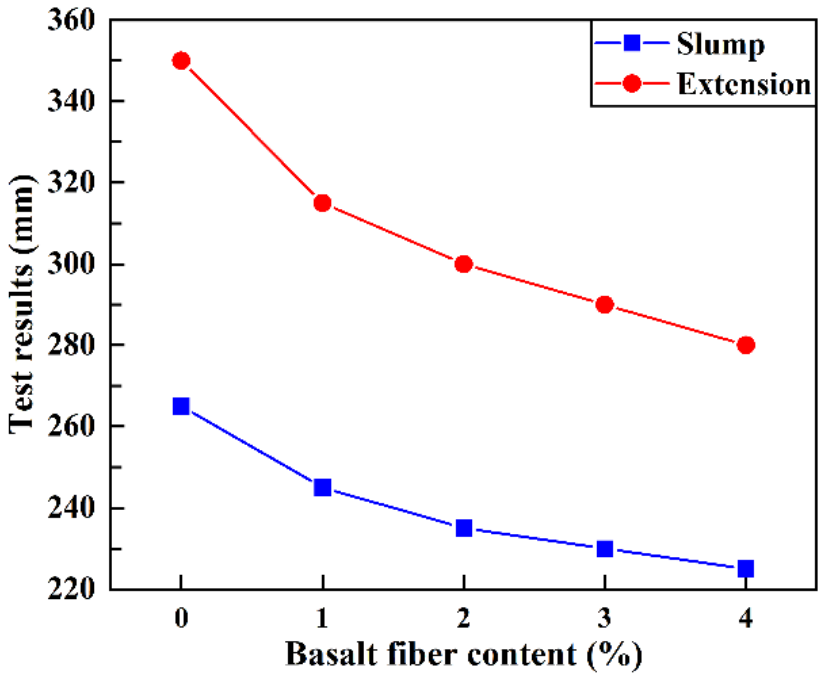


**Figure 5.** The test results of slump and extension.

### 3.1.2. Failure Mode

The compressive failure mode of BFRPC is shown in Figure 6. The RPC failure form without BF is brittle failure. When BF was added, the specimen surface still exhibited slight peeling accompanied by a number of small cracks. This phenomenon occurred because the friction between BF and the matrix limits the development of cracks and maintain integrity after any damaging event.

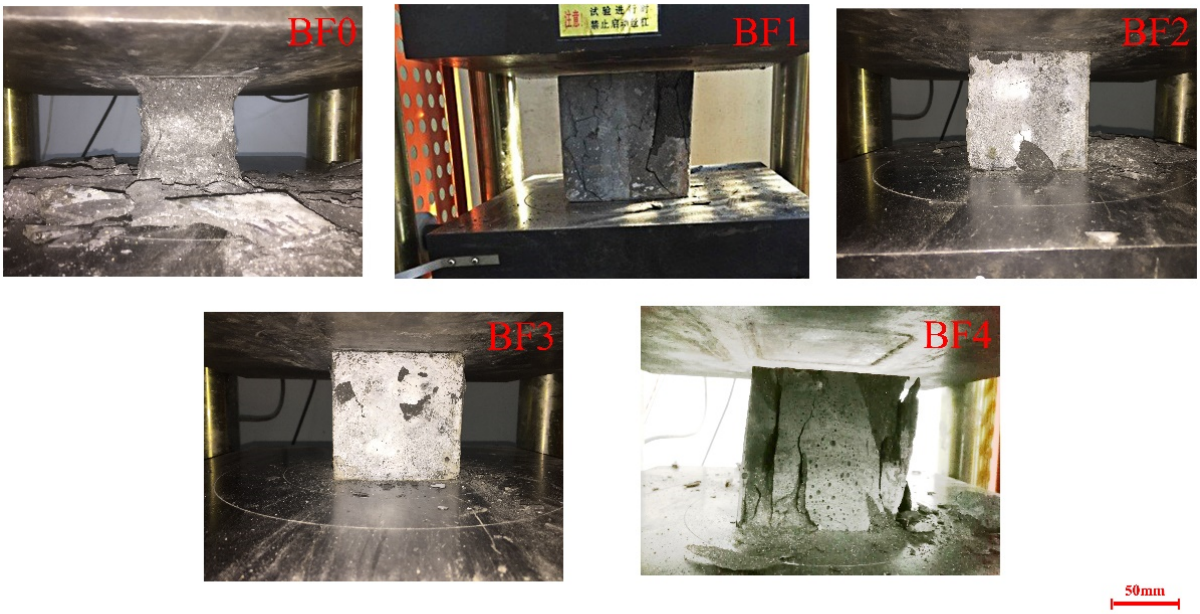


**Figure 6.** Compressive strength failure mode.

The failure modes of BFRPC splitting tensile strength are shown in Figure 7. The cracks of the RPC without BF gradually developed and penetrated along the middle of the specimen due to the longitudinal splitting failure form. When mixed with BF, the basic crack interface was a flat line because the BF incorporation can have similar "reinforcement" effect. In the event of a micro crack, the BF and matrix under tensile stress showed plastic failure, effectively improving the toughness of BFRPC.

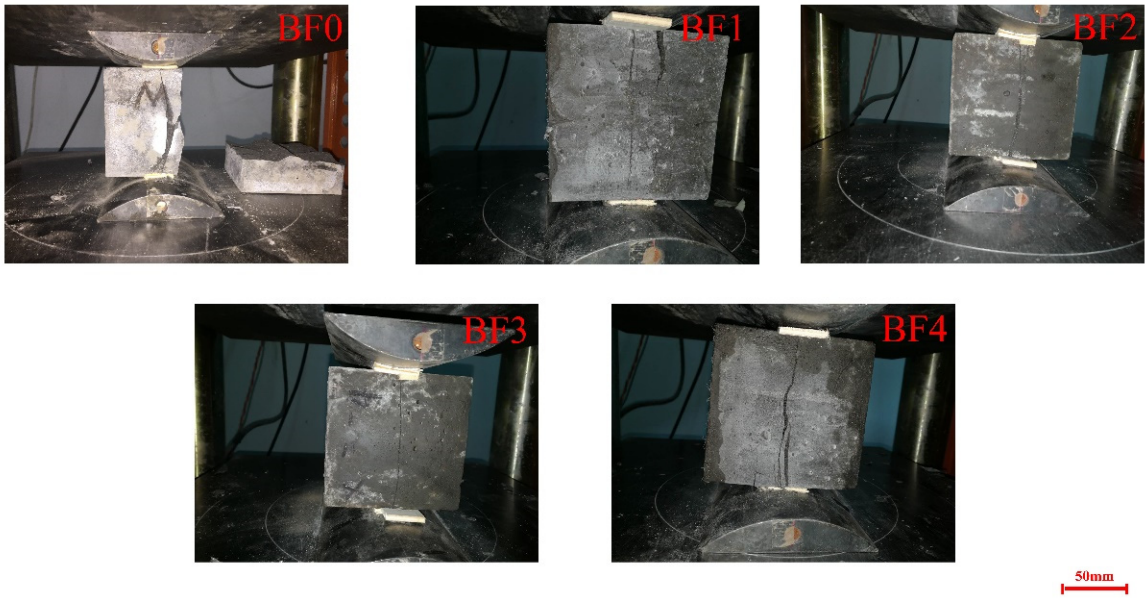


**Figure 7.** Splitting tensile strength failure mode.

B. Ramesh [64] and Zhang [65] obtained similar results. When BF was not doped, with the gradual increase in load, the cracks expanded rapidly, and a loud cracking sound was made when the compressive strength test was damaged, and the damage was in the form of quadrangular cone damage, and the splitting tensile strength test was suddenly split into two halves when the ultimate load was reached. After the incorporation of BF, due to

the bridging effect of fiber on the cracks effectively limiting the expansion of cracks, the specimens show good plasticity. Therefore, BF can improve the crack resistance of concrete.

#### 3.1.3. Analysis of Mechanical Properties

The test results of 7- and 28-day compressive strength and splitting tensile strength of BFRPC are shown in Figures 8 and 9. When the amount of BF is 2 kg/m$^3$, it is the best amount. The maximum compressive strength at 28-day reaches 95.2 MPa and the maximum splitting tensile strength reaches 7.78 MPa. With the increase in the amount of BF, the mechanical properties of BFRPC gradually decreases. When the content of BF is low, it can be evenly distributed in the mixture, forming a dense spatial network structure with the aggregate, optimizing the internal structure, reducing the internal porosity, and creating a homogeneous and complete structural system. When cracks occur, BF can play a bridging role and effectively prevent the development of cracks. However, when the content of BF exceeds the optimum content, the BF clumps in the matrix, affects the overall uniformity of the mixture, forms many weak surfaces, and fails to generate a space grid with integrity, resulting in the declining trend of the strength of BFRPC.

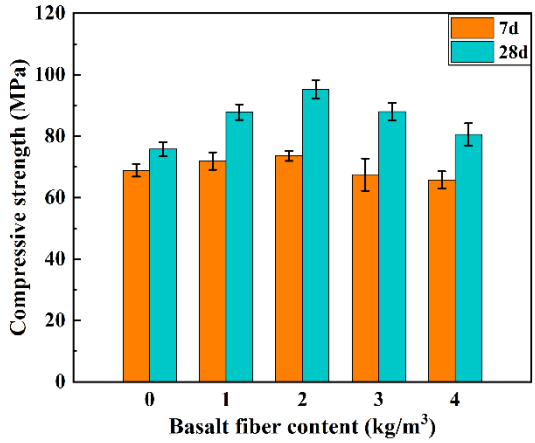


**Figure 8.** Compressive strength.

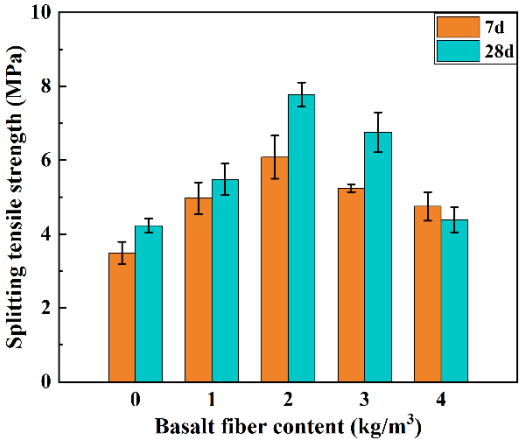


**Figure 9.** Splitting tensile strength.

The effect of BF on the improvement of compressive strength of RPC was not significant. When the dosage was 2 kg/m$^3$, the compressive strength increased the most, and the maximum increase percentage was 6.84% and 25.70% at 7 and 28 days, respectively. The splitting tensile strength of RPC increased by BF was large. When the dosage was 2 kg/m$^3$, the maximum increase in splitting tensile strength was 74.21% and 83.92% for 7 and 28 days, respectively. BF can improve the strength of RPC because BF has excellent

material properties. Hence, a complete bearing system is formed between the aggregates. When the BFRPC is loaded, the BF at the stress concentration point acts as a bridge, thus, effectively limiting the initiation and expansion of the crack and improving the mechanical properties of BFRPC.

As found in earlier studies, the addition of BF can improve the compressive strength [55] and splitting tensile strength [66] of concrete, but the improvement of compressive strength is not obvious [67]. Zhang [68] also showed that BF added to concrete was more effective in enhancing tensile and flexural strengths than compressive strength. Liu [56] pointed out that uniformly distributed BF can inhibit crack sprouting and bear part of the load, thus, increasing the compressive strength. Sha [67] pointed out that BF effectively inhibited the extension of microcracks, mainly due to the bridging effect of randomly distributed discrete fiber on the cracks. After bending cracking, the stress is transferred to the bridging fiber, which retards the crack development and increases the cracking tensile strength. The conclusions of these studies are the same as the results of this study.

### *3.2. Microstructure Analysis of BFRPC*

#### 3.2.1. SEM Characterization Analysis

The microscopic morphology and fiber distribution of BFRPC were analyzed by SEM, and the BF reinforcement mechanism was further analyzed through the microstructure.

From the microstructure, the BF is tightly bonded to the substrate and no interfacial transition zone is observed. When BFRPC is under the action of external load, BF is closely connected to the substrate and shares the stress with the substrate. The two use their own strength and good interfacial adhesion to absorb the energy of crack development, which effectively inhibits the development of cracks and achieves the purpose of toughening and blocking the crack of concrete, so that the microstructure of concrete can be improved and eventually be pulled out or fractured. Figure 10a shows the smooth hole left after the fiber is pulled out from the matrix, and Figure 10b shows the cross section of the broken fiber. As demonstrated in the Zhang [65] study, when the BF content is small, most of the BF distributed along the crack is pulled out or broken, and when the BF content is sufficient, the fiber can withstand most of the transverse tensile force, slowing down the stress concentration and effectively preventing the crack expansion and development. However, as shown in Figure 10a, when BF is added in excess, the fiber will agglomerate and overlap due to the uneven distribution of BF, which affects the degree of bonding between the cementitious base and the interfacial transition zone, leading to a decrease in the contribution of BF to the improvement of mechanical properties. Sha [67] also pointed out in his study that when the volume fraction of BF is too high it will agglomerate, leading to a decrease in compressive strength.

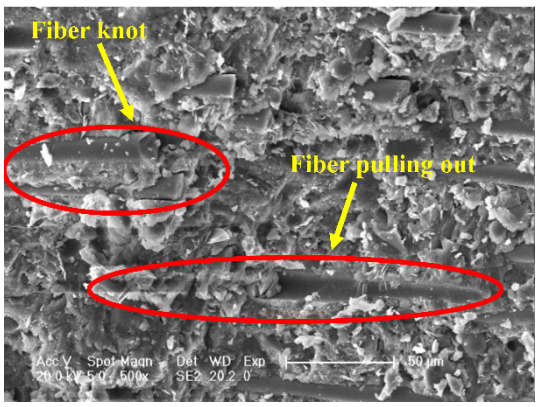


(**a**) Fiber overlap and pulling out

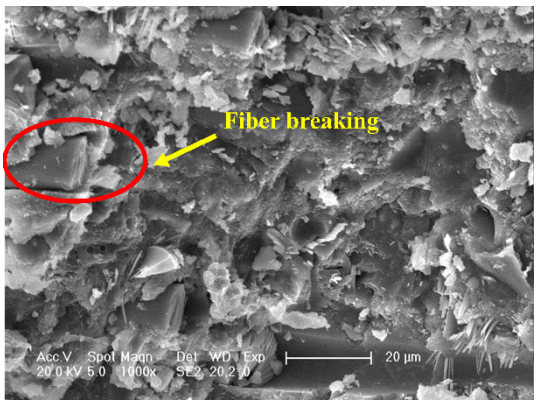


(**b**) Fiber breaking

**Figure 10.** BFRPC microstructure.

3.2.2. Quantitative Analysis of Microstructure

Concrete is a porous composite material. As an important part of the microstructure, aggregate particles and pore structure characteristics have a significant impact on the macroscopic mechanical properties of concrete [69,70]. Therefore, Image-Pro Plus image processing software was used for quantitative analysis of the microstructure parameters of BFRPC. The fractal dimension reflects the effectiveness of the space occupied by the complex shape, and it is a measure of the irregularity of the complex shape. Abundance refers to the ratio of the short axis to the long axis of the particle or pore, which indicates the geometric shape characteristics of the particle or pore, with the value of abundance tending to 0, the particle or pore is similar to a long strip; with the value of abundance tending to 1, the particle or pore tends to be equiaxed. Roundness characterizes the degree of particle or pore approximating to standard circle; the larger the value of roundness, the more the particle or pore approximates to the circle. The distribution results of particle size and pore size are shown in Figures 11 and 12, and the microscopic parameter results of particle and pore are shown in Figures 13 and 14.

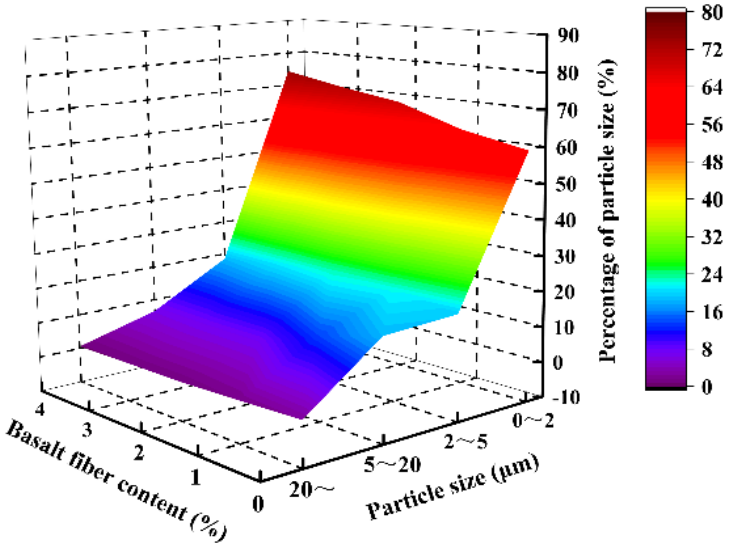


**Figure 11.** Particle size distribution.

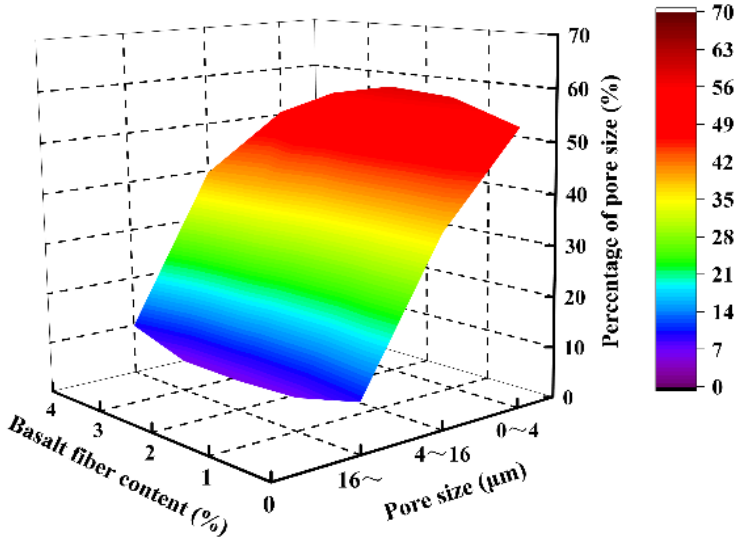


**Figure 12.** Pore size distribution.

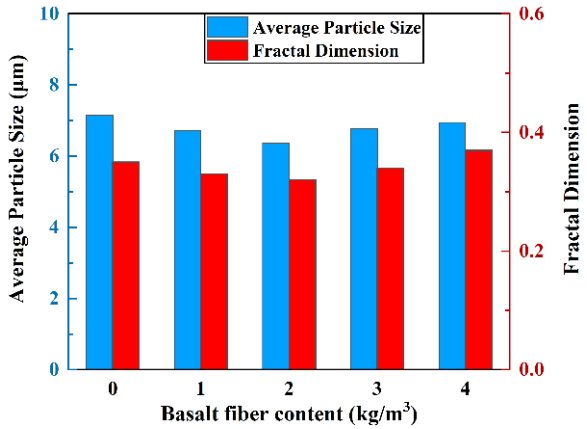


(**a**) Average particle size and fractal dimension

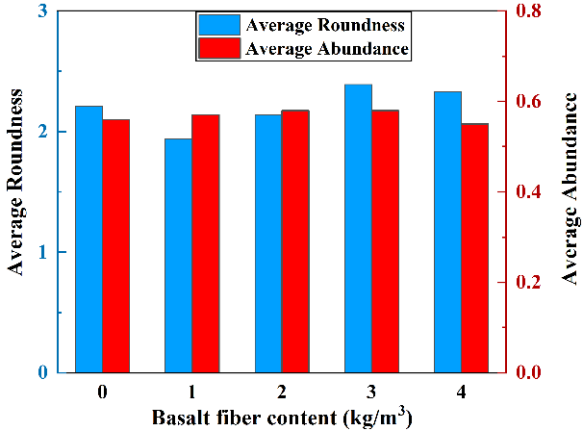


(**b**) Average roundness and abundance

**Figure 13.** Particle microparameters.

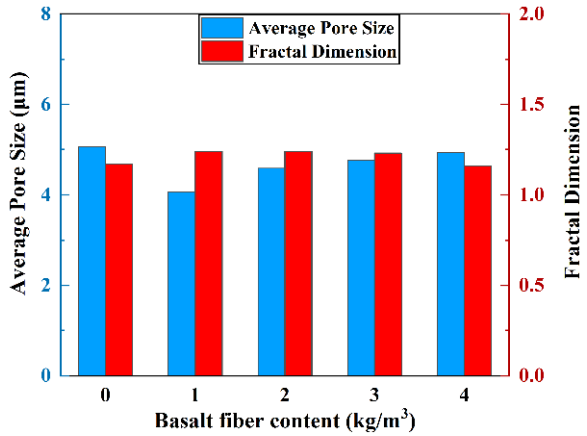


(**a**) Average pore size and fractal dimension

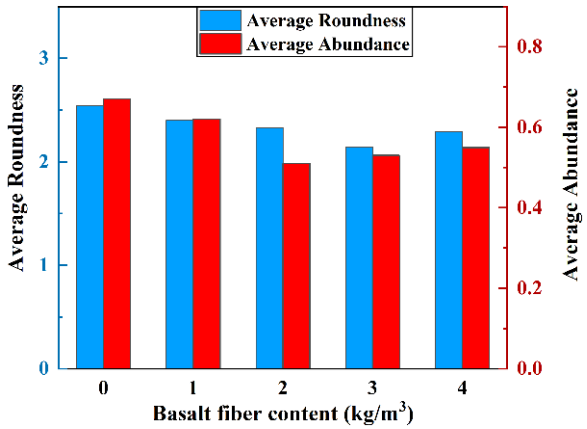


(**b**) Average roundness and abundance

**Figure 14.** Pore microparameters.

Figure 11 shows that in BFRPC, the particle size was mostly 0–2 μm. The content of particles larger than 20 μm was small. With the increase in the content of BF, the content of 0–2 μm particles gradually increased, that of 2–5 μm particles increased first and then decreased, and that of 5–20 μm and >20 μm particles gradually decreased when the content of BF was 2 kg/m$^3$.

As shown in Figure 12, the content of 0–4 μm pores in BFRPC was high, and that of >16 μm pores was less. With the increase in BF addition, the content of 0–4 μm pores first increased, then decreased, and was maximized when the BF addition was 2 kg/m$^3$. When the content of BF is small, it can be distributed evenly in the RPC, effectively improving the generation of pores and cracks in RPC and reducing the porosity in BFRPC. The pore size larger than 4μm tends to decrease first and then increase, and it is the smallest, with a content of 2 kg/m$^3$. This is due to the high content of BF, which leads to uneven distribution of BF, resulting in the agglomeration and increased internal porosity of BFRPC.

The particle microparameters are shown in Figure 13. With the increase in BF content, the particle area ratio did not change but was the largest when the content was 2 kg/m$^3$. The average particle size and fractal dimension of particle size gradually decrease when the fiber content is 0–2 kg/m$^3$ and gradually increase when the fiber content is 2–4 kg/m$^3$. The average abundance of particles basically increased first and then decreased, and the average circularity of particles showed no change. As can be seen in Figure 14, with the increase in BF content, the pore area ratio and average pore abundance gradually decrease when the

fiber content is 0–2 kg/m$^3$, and gradually increase when the fiber content is 2–4 kg/m$^3$. The average pore size and average pore roundness showed no change, and the fractal dimension of pores basically increased first and then decreased. The fractal dimension of BFRPC pores is the same and maximum at the dosing of 1 kg/m$^3$ and 2 kg/m$^3$.

Xu [54] pointed out through the analysis of the microstructure of concrete that the incorporation of fiber can effectively improve the internal structure of concrete, making the particles and pores smaller, uniform, complex, and full. BF achieves an enhanced toughening effect by connecting the matrix into a whole, mainly through its own strength and good interfacial adhesion.

#### 3.2.3. Gray Correlation Analysis

Gray correlation analysis method can not only solve the conventional and irregular sample size but also reduce the calculation amount, which is a convenient and efficient analysis method [71]. Some scholars studied the strength prediction of recycled aggregate concrete and factors affecting properties of cement-based composites by using gray correlation analysis and achieved good results [72,73].

Gray correlation analysis was used to analyze the BFRPC macro mechanical properties and microstructure parameters, calculate the correlation values between macroscopic mechanical properties and microscopic parameters, and determine the main factors influencing the mechanical properties BFRPC. The gray correlation calculation results are shown in Tables 4 and 5.

**Table 4.** The correlation value of particle morphology with strength.

| Particle Microscopic Parameter | | Area Ratio | Average Particle Size | Fractal Dimension | Average Roundness | Average Abundance |
|---|---|---|---|---|---|---|
| Correlation degree | Compressive strength | 0.730 | 0.572 | 0.522 | 0.484 | 0.743 |
| | Splitting tensile strength | 0.646 | 0.599 | 0.614 | 0.611 | 0.635 |

**Table 5.** The correlation value of pore structure with strength.

| Pore Microscopic Parameter | | Area Ratio | Average Pore Size | Fractal Dimension | Average Roundness | Average Abundance |
|---|---|---|---|---|---|---|
| Correlation degree | Compressive strength | 0.536 | 0.577 | 0.815 | 0.660 | 0.589 |
| | Splitting tensile strength | 0.637 | 0.663 | 0.733 | 0.665 | 0.617 |

Table 4 shows that the correlation between particle microscopic parameters and BFRPC compressive strength was in the order of primary and secondary: particle area ratio > average abundance > average particle size > fractal dimension > average roundness. However, only the correlation between particle area ratio and average particle abundance and compressive strength exceeded 0.6, indicating that the particle area ratio and average particle abundance have a significant effect on BFRPC. In addition, the order of correlation between particle microscopic parameters and the splitting tensile strength of BFRPC was as follows: particle area ratio > average abundance > particle fractal dimension > average roundness > average particle size. The correlation values between particle area ratio, particle average abundance, particle fractal dimension, particle roundness, and splitting tensile strength were all greater than 0.6, and the correlation value between average particle size and splitting tensile strength was 0.599, which was close to 0.6. This finding indicates that the microcosmic parameters of particles are closely related to the splitting tensile strength of BFRPC.

Table 5 shows the primary and secondary relationship between pore microscopic parameters and BFRPC compressive strength is as follows: pore fractal dimension > average porosity roundness > average porosity abundance > average pore size > pore area ratio, but only the correlation between pore fractal dimension and average porosity roundness and compressive strength is more than 0.6, indicating that the fractal dimension and

average porosity roundness have a significant effect on BFRPC. In addition, the primary and secondary relationship between pore microscopic parameters and the splitting tensile strength of BFRPC is as follows: pore fractal dimension > average roundness > average pore size > pore area ratio > average abundance, and the correlation values of all pore microscopic parameters and splitting tensile strength are greater than 0.6, indicating that the pore microscopic parameters are closely related to the splitting tensile strength of BFRPC.

As Xu [54] showed by analyzing the micro parameters and macro strength of concrete through gray correlation, compared with compressive strength, micro parameters have a closer correlation with splitting tensile strength.

## 4. BFRPC Strength Calculation Formula

Statistical and mathematical models have been applied to the study of cementitious composites. An increasing number of scholars have investigated concrete strength prediction models, of which regression analysis is the most widely used method. Gao [74] developed regression formula for compressive strength and critical strain for steel fiber reinforced recycled coarse aggregate concrete. Zhong [26] proposed formulas for calculating the manufactured sand RPC compressive strength and splitting tensile strength using regression analysis, and the applicability of the formulas was verified and discussed. Kazmi [75] proposed an empirical formula between fiber admixture and post-peak behavior. In these studies, correlations between performance indicators and factors were investigated using linear or nonlinear regression models.

The strength calculation formula of BFRPC is obtained by fitting the test results of mechanical properties of BFRPC. The contribution of BF to compressive strength $\lambda_c$ and splitting tensile strength $\lambda_t$ were obtained by fitting the percentage increase in compressive strength and percentage increase in splitting tensile strength of BFRPC in 28 days, respectively. The calculation formula is shown in Figure 15. Since BF has a negative effect on BFRPC when it exceeds 2 kg/m$^3$, according to the percentage of improvement of mechanical properties of BFRPC by the content of BF between 0 and 4 kg/m$^3$. The strength calculation formula of BFRPC with BF content of 0–4 kg/m$^3$ is proposed:

$$f_c = f_{c0}\,(1 + \lambda_c) \tag{1}$$

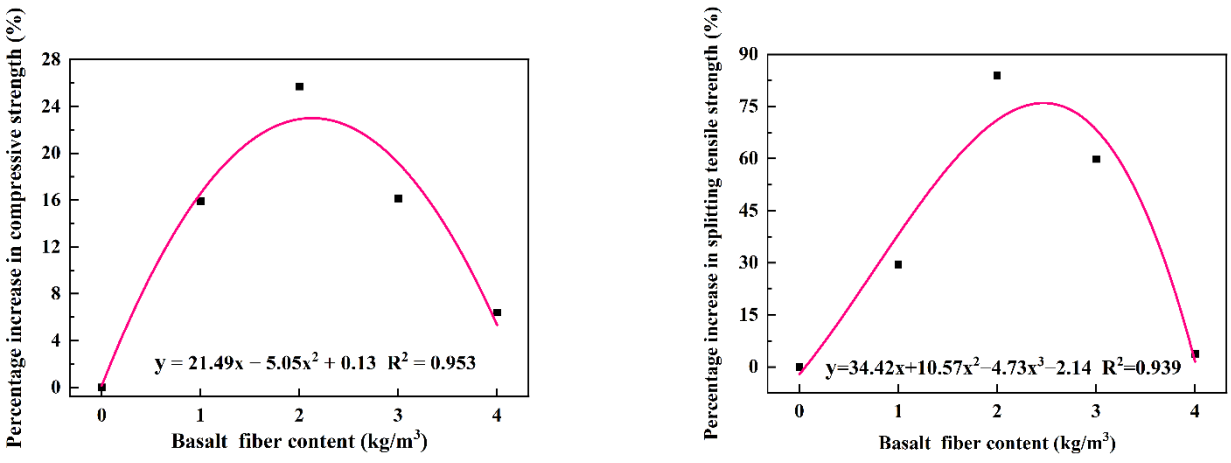


(**a**) compressive strength (**b**) splitting tensile strength

**Figure 15.** Relationship between BF content and mechanical properties.

In the formula: $f_c$ is 28-day compressive strength (MPa), $\lambda_c$ is contribution rate of compressive strength with different BF content, $f_{c0}$ is compressive strength when BF content is 0 kg/m$^3$ (MPa).

$$f_t = f_{t0}\,(1 + \lambda_t) \tag{2}$$

In the formula: $f_t$ is 28-day splitting tensile strength (MPa), $\lambda_t$ is contribution rate of splitting tensile strength with different BF content, $f_{t0}$ is splitting tensile strength when BF content is 0 kg/m$^3$ (MPa).

In order to make the BFRPC strength calculation formula widely used, the prediction formula is used to calculate the strength of BFRPC with different BF content in this study. The calculation results and errors are shown in Table 6, and the comparison between the calculated value and the test value is shown in Figure 16. The maximum error between the calculated value of compressive strength and the test value is 2.59%, and the maximum error between the calculated value of splitting tensile strength and the test value is 6.95%, and the errors are all within 10%. Therefore, this calculation formula has certain reference value.

**Table 6.** The experimental results are compared with those calculated by the calculation formula.

| BF Content (kg/m$^3$) | Compressive Strength | | | | Splitting Tensile Strength | | | |
|---|---|---|---|---|---|---|---|---|
| | $\lambda_c$ (%) | Calculation Value (MPa) | Experimental Value (MPa) | Error (%) | $\lambda_t$ (%) | Calculation Value (MPa) | Experimental Value (MPa) | Error (%) |
| 0 | 0.12 | 75.87 | 75.77 | 0.13 | −2.14 | 4.14 | 4.23 | −2.14 |
| 1 | 16.51 | 88.33 | 87.82 | 0.58 | 38.12 | 5.84 | 5.48 | 6.61 |
| 2 | 22.84 | 93.13 | 95.24 | −2.22 | 71.14 | 7.24 | 7.78 | −6.95 |
| 3 | 19.11 | 90.28 | 88.00 | 2.59 | 68.54 | 7.13 | 6.76 | 5.46 |
| 4 | 5.32 | 79.78 | 80.61 | −1.03 | 1.94 | 4.31 | 4.39 | −1.78 |

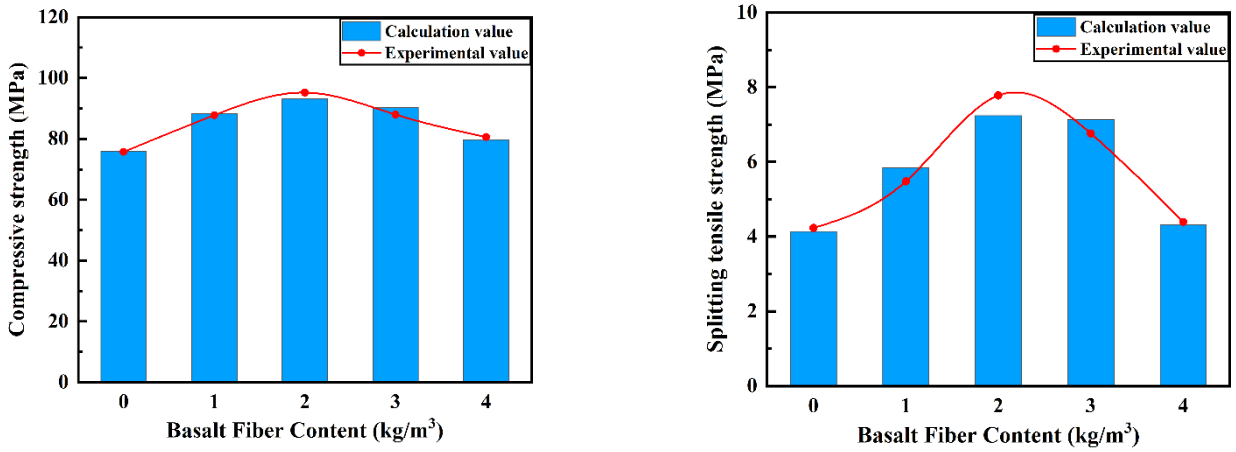


(**a**) Compressive strength (**b**) Splitting tensile strength

**Figure 16.** The experimental results are compared with those calculated by the calculation formula.

Dong and Shen et al. studied the compressive strength of BFRPC 28-day mixed with 0, 2, 3, 4, 5 kg/m$^3$ [76,77]. The test results of Dong [76] and Shen [77] were encoded into Formula (1) for calculation to further verify the feasibility and applicability of the strength calculation formula. The comparison of calculated and experimental values is shown in Table 7. Only a few reports are available on the splitting tensile strength of BFRPC, and different BF sizes have a great impact on the splitting tensile strength. Therefore, other research results cannot be better used to verify the calculation formula.

As shown in Figure 17, the calculation results obtained by using the BFRPC strength calculation formula are very close to the actual test results, and the error is very small, all within 15%, and the maximum error is 14.65%. Therefore, this model can better predict the mechanical properties of 28-day BFRPC, with BF content between 0–4 kg/m$^3$ and predict the strength of BFRPC in advance, according to the fiber content, which has a guiding role for the further research and application of BFRPC.

**Table 7.** The experimental results of Dong [76] and Shen [77] were compared with those calculated by the calculation formula.

| BF Content ($kg/m^3$) | $\lambda_c$ (%) | Compressive Strength of Dong [76] | | | Compressive Strength of Shen [77] | | |
|---|---|---|---|---|---|---|---|
| | | Calculation Value (MPa) | Experimental Value (MPa) | Error (%) | Calculation Value (MPa) | Experimental Value (MPa) | Error (%) |
| 0 | 0.13 | 86.11 | 86 | 0.13 | 85.70 | 85.60 | 0.13 |
| 2 | 22.91 | 105.70 | 101 | 4.66 | 105.21 | 100.5 | 4.68 |
| 3 | 19.15 | 102.47 | 115 | −10.90 | 101.99 | 115.2 | −11.46 |
| 4 | 5.29 | 90.55 | 106 | −14.58 | 90.13 | 105.6 | −14.65 |

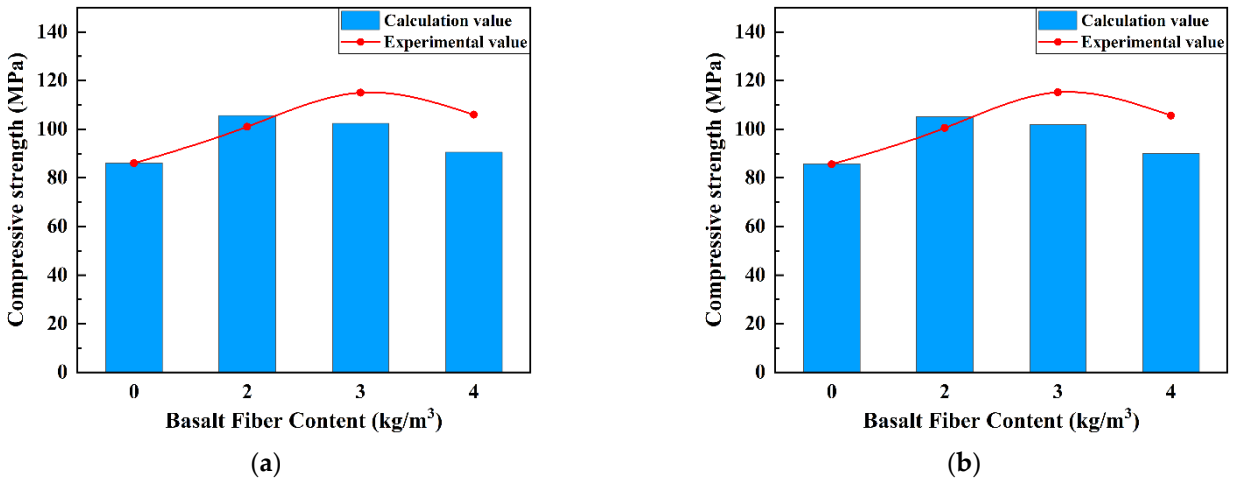


**Figure 17.** The experimental results of (**a**) Dong [76] and (**b**) Shen [77] were compared with those calculated by the calculation formula.

## 5. Conclusions

- The strength of BFRPC tends to decrease when the BF content exceeds 2 $kg/m^3$. When BF content is at 2 $kg/m^3$, the 28-day compressive strength reaches 95.2 MPa and splitting tensile strength reaches 7.78 MPa.
- BF can closely bond to the matrix without forming a transition zone. The energy of crack development is absorbed by the bridging and interfacial bond force, thus, effectively inhibiting the development of crack and improving the mechanical properties of BFRPC. However, when BF is added in excess, agglomeration and overlapping will occur and reduce the mechanical properties of BFRPC.
- The incorporation of BF can improve the microstructure of BFRPC, reduce the size of particles and pores, and provide a uniform and plump morphology of particles and pores. When the BF content is 2 $kg/m^3$, the particle area ratio and pore area ratio are the lowest. When the content of BF is too high, the internal porosity is increased due to the uneven mixing of the fiber. Based on the gray correlation analysis method, it was concluded that the particle area ratio and pore fraction dimension were the most correlated with the mechanical properties of BFRPC.
- The strength calculation formula can be used to effectively obtain RPC compressive strength and splitting tensile strength with different BF content, so as to check whether the design fiber content can meet the target actual engineering requirements, and the fiber content can be flexibly selected, according to the required strength. This work serves as a reliable reference for the engineering application of BFRPC.
- Limitation: Different fiber types, sizes, and curing methods have different effects on the mechanical properties of RPC. Therefore, the strength calculation formula proposed in this paper is only applicable when the raw materials and curing methods are the same as this study, and the calculated values for different materials and curing methods will have different degrees of deviation from the actual values, and the use of this method is not recommended.

- Future direction: On the basis of this study, further research on the durability performance and damage mechanism of BFRPC is proposed to be carried out in the future to provide valuable references for improving structural safety and extending service life.

**Author Contributions:** Conceptualization, M.L. and W.D.; methodology, M.L. and W.D.; software, M.L. and X.Y.; validation, M.L. and C.Z.; formal analysis, M.L., W.D. and C.Z.; investigation, M.L. and X.Y.; resources, W.D. and C.Z.; data curation, M.L. and C.Z.; writing—original draft preparation, M.L.; writing—review and editing, M.L. and W.D.; visualization, C.Z. and X.Y.; supervision, W.D. and C.Z.; project administration, W.D.; funding acquisition, W.D. All authors have read and agreed to the published version of the manuscript.

**Funding:** This study was funded by the Jilin Scientific and Technological Development Program (20190303033SF).

**Data Availability Statement:** The data presented in this study are available on request from the corresponding author. The data are proprietary or confidential in nature and may only be provided with restrictions.

**Acknowledgments:** The authors would like to thank the anonymous reviewers for their constructive suggestions and comments to improve the quality of the paper.

**Conflicts of Interest:** The authors declare no conflict of interest.

## References

1. Richard, P.; Cheyrezy, M. Composition of reactive powder concretes. *Cem. Concretce Res.* **1995**, *25*, 1501–1511. [CrossRef]
2. Cheyrezy, M.; Maret, V.; Frouin, L. Microstructural analysis of RPC (Reactive Powder Concrete). *Cem. Concr. Res.* **1995**, *25*, 1491–1500. [CrossRef]
3. Hiremath, P.N.; Yaragal, S.C. Effect of different curing regimes and durations on early strength development of reactive powder concrete. *Constr. Build. Mater.* **2017**, *154*, 72–87. [CrossRef]
4. Ahmad, S.; Zubair, A.; Maslehuddin, M. Effect of key mixture parameters on flow and mechanical properties of reactive powder concrete. *Constr. Build. Mater.* **2015**, *99*, 73–81. [CrossRef]
5. Mostofinejad, D.; Nikoo, M.R.; Hosseini, S.A. Determination of optimized mix design and curing conditions of reactive powder concrete (RPC). *Constr. Build. Mater.* **2016**, *123*, 754–767. [CrossRef]
6. Qin, R.; Xhb, C.; Chao, G. Quantifying curing and composition effects on compressive and tensile strength of 160–250MPa RPC. *Constr. Build. Mater.* **2020**, *241*, 117987.
7. Mao, X.Q.; Qu, W.; Zhu, P. Mixture Optimization of Green Reactive Powder Concrete with Recycled Powder. *J. Mater. Civ. Eng.* **2019**, *31*, 04019033.1–04019033.11. [CrossRef]
8. Xu, X.; Zhang, R.; Liu, Y. Influence of curing regime on properties of reactive powder concrete containing waste steel fibers-ScienceDirect. *Constr. Build. Mater.* **2020**, *232*, 117129.
9. Kannan, R.; Mathangi, D.P.; Sudha, C.; Neelamegam, M. Experimental Investigation of Reactive Powder Concrete exposed to Elevated Temperatures. *Constr. Build. Mater.* **2020**, *261*, 119593.
10. Zdeb, T. An analysis of the steam curing and autoclaving process parameters for reactive powder concretes. *Constr. Build. Mater.* **2017**, *131*, 758–766. [CrossRef]
11. Alharbi, Y.R.; Abadel, A.A.; Mayhoub, O.A.; Kohail, M. Effect of using available metakaoline and nano materials on the behavior of reactive powder concrete. *Constr. Build. Mater.* **2020**, *269*, 121344. [CrossRef]
12. Rahmatabadi, M.A.D. Mechanical properties of reactive powder concrete under pre-setting pressure and different curing regimes. *J. Str. Civ. Eng. Res.* **2015**, *4*, 354–358. [CrossRef]
13. Effects of high-pressure/temperature curing on reactive powder concrete microstructure formation. *Constr. Build. Mater.* **2016**, *105*, 554–562. [CrossRef]
14. Lei, W.; Th, A.; Yz, C.; Tang, S.; Tan, J.; Liu, Z.; Su, J. The influence of fiber type and length on the cracking resistance, durability and pore structure of face slab concrete-ScienceDirect. *Constr. Build. Mater.* **2021**, *282*, 122706.
15. Wang, L.; Guo, F.; Yang, H.; Wang, Y.; Tang, S. Comparison of Fly Ash, Pva Fiber, Mgo and Shrinkage-Reducing Admixture on the Frost Resistance of Face Slab Concrete via Pore Structural and Fractal Analysis. *Fractals* **2021**, *29*, 2140002. [CrossRef]
16. Wang, H.; Shi, F.; Shen, J.; Zhang, A.; Zhang, L.; Huang, H.; Liu, J.; Jin, K.; Feng, L.; Tang, Z. Research on the self-sensing and mechanical properties of aligned stainless steel fiber-reinforced reactive powder concrete. *Cem. Concr. Compos.* **2021**, *119*, 104001. [CrossRef]
17. Chen, X.; Wan, D.W.; Jin, L.Z.; Qian, K.; Fu, F. Experimental studies and microstructure analysis for ultra high-performance reactive powder concrete. *Constr. Build. Mater.* **2019**, *229*, 116924.1–116924.15. [CrossRef]
18. Xu, Z.; Hao, H.; Li, H.N. Experimental study of dynamic compressive properties of fibre reinforced concrete material with different fibres. *Mater. Des.* **2012**, *33*, 42–55. [CrossRef]

19. Han, B.; Dong, S.; Ou, J.; Zhang, C.; Wang, Y.; Yu, X.; Ding, S. Microstructure related mechanical behaviors of short-cut super-fine stainless wire reinforced reactive powder concrete. *Mater. Des.* **2016**, *96*, 16–26. [CrossRef]
20. Vigneshwari, M.; Arunachalam, K.; Angayarkanni, A. Replacement of silica fume with thermally treated rice husk ash in Reactive Powder Concrete. *J. Clean. Prod.* **2018**, *188*, 264–277. [CrossRef]
21. Al-Tikrite, A.; Hadi, M. Mechanical properties of reactive powder concrete containing industrial and waste steel fibres at different ratios under compression. *Constr. Build. Mater.* **2017**, *154*, 1024–1034. [CrossRef]
22. Chen, M.; Zheng, W. A Study on Optimum Mixture Ratio of Reactive Powder Concrete. *Adv. Mater. Sci. Eng.* **2018**, *2018*, 1–7. [CrossRef]
23. Zhong, C.; Liu, M.; Zhang, Y.; Wang, J.; Liang, D.; Chang, L. Study on Mechanical Properties of Hybrid Polypropylene-Steel Fiber RPC and Computational Method of Fiber Content. *Materials* **2020**, *13*, 2243. [CrossRef] [PubMed]
24. Khalil, W.; Damha, L.S. Mechanical properties of reactive powder concrete with various steel fiber and silica fume contents. *ACTA Tec. Corviniensis Bull. Eng.* **2014**, *7*, 47–58.
25. Mizani, J.; Sadeghi, A.M.; Afshin, H. Experimental study on the effect of macro and microfibers on the mechanical properties of reactive powder concrete. *Struct. Concr.* **2022**, *23*, 240–254. [CrossRef]
26. Zhong, C.; Liu, M.; Zhang, Y.; Wang, J. Study on mix proportion optimization of manufactured sand RPC and design method of steel fiber content under different curing methods. *Materials* **2019**, *12*, 1845. [CrossRef] [PubMed]
27. Dong, S.; Dong, X.; Ashour, A.; Han, B.; Ou, J. Fracture and self-sensing characteristics of super-fine stainless wire reinforced reactive powder concrete-ScienceDirect. *Cem. Concr. Compos.* **2020**, *105*, 103427. [CrossRef]
28. Dong, S.; Zhou, D.; Ashour, A.; Han, B.; Ou, J. Flexural toughness and calculation model of super-fine stainless wire reinforced reactive powder concrete. *Cem. Concr. Compos.* **2019**, *104*, 103367. [CrossRef]
29. Wang, H.; Gao, X.; Liu, J.; Ren, M.; Lu, A. Multi-functional properties of carbon nanofiber reinforced reactive powder concrete. *Constr. Build. Mater.* **2018**, *187*, 699–707. [CrossRef]
30. Raza, S.S.; Qureshi, L.A. Effect of carbon fiber on mechanical properties of reactive powder concrete exposed to elevated temperatures. *J. Build. Eng.* **2021**, *42*, 102503. [CrossRef]
31. Raza, S.S.; Qureshi, L.A.; Ali, B.; Raza, A.; Khan, M.M. Effect of different fibers (steel fibers, glass fibers, and carbon fibers) on mechanical properties of reactive powder concrete. *Struct. Concr.* **2020**, *22*, 334–346. [CrossRef]
32. Kizilkanat, A.B.; Kabay, N.; Akyuncu, V.; Chowdhury, S.; Akça, A.H. Mechanical properties and fracture behavior of basalt and glass fiber reinforced concrete: An experimental study. *Constr. Build. Mater.* **2015**, *100*, 218–224. [CrossRef]
33. Özkan, Ş.; Demir, F. The hybrid effects of PVA fiber and basalt fiber on mechanical performance of cost effective hybrid cementitious composites-ScienceDirect. *Constr. Build. Mater.* **2020**, *263*, 120564. [CrossRef]
34. Xu, M.; Song, S.; Feng, L.; Zhou, J.; Li, H.; Li, V.C. Development of basalt fiber engineered cementitious composites and its mechanical properties. *Constr. Build. Mater.* **2021**, *266*, 121173. [CrossRef]
35. Zhang, H.; Wang, B.; Xie, A.; Qi, Y. Experimental study on dynamic mechanical properties and constitutive model of basalt fiber reinforced concrete. *Constr. Build. Mater.* **2017**, *152*, 154–167. [CrossRef]
36. Dna, B.; Li, S.B.; Yang, L.B.; Huang, D.; Luo, D. Experimental study on mechanical properties and durability of basalt fiber reinforced coral aggregate concrete. *Constr. Build. Mater.* **2020**, *237*, 117628.
37. Khan, M.; Cao, M.; Xie, C.; Ali, M. Hybrid fiber concrete with different basalt fiber length and content. *Struct. Concr.* **2022**, *23*, 346–364. [CrossRef]
38. Dilbas, H.; Akr, Z. Influence of basalt fiber on physical and mechanical properties of treated recycled aggregate concrete. *Constr. Build. Mater.* **2020**, *254*, 119216. [CrossRef]
39. Zhou, H.; Jia, B.; Huang, H.; Mou, Y. Experimental Study on Basic Mechanical Properties of Basalt Fiber Reinforced Concrete. *Materials* **2020**, *13*, 1362. [CrossRef]
40. Khan, M.; Cao, M.; Xie, C.; Ali, M. Effectiveness of hybrid steel-basalt fiber reinforced concrete under compression. *Case Stud. Constr. Mater.* **2022**, *16*, e00941. [CrossRef]
41. Wang, D.; Ju, Y.; Shen, H.; Xu, L. Mechanical properties of high performance concrete reinforced with basalt fiber and polypropylene fiber. *Constr. Build. Mater.* **2019**, *197*, 464–473. [CrossRef]
42. Ding, Y.H.; Guo, S.Q.; Zhang, X.G. Influence of basalt fiber on the anti-carbonation performance of recycled aggregate concrete. *Acta Mater. Compos. Sin.* **2022**, *39*, 1228–1238. (In Chinese)
43. Lu, L.; Han, F.; Wu, S.; Qin, Y.; Yuan, G.; Doh, J.-H. Experimental study on durability of basalt fiber concrete after elevated temperature. *Struct. Concr.* **2021**, *23*, 682–693. [CrossRef]
44. Jin, M.; Jiang, L.; Lu, M.; Bai, S. Monitoring chloride ion penetration in concrete structure based on the conductivity of graphene/cement composite. *Constr. Build. Mater.* **2017**, *136*, 394–404. [CrossRef]
45. Moffatt, E.G.; Thomas, M.; Fahim, A. Performance of high-volume fly ash concrete in marine environment. *Cem. Concr. Res.* **2017**, *102*, 127–135. [CrossRef]
46. Wang, Z.-S.; Li, Y.-K.; Lu, J.-L.; Tian, J.-B.; Zhao, K. Research on Corrosion Characteristics and Performance Degradation of Basalt Fiber Concrete under Sodium Magnesium Sulfate Corrosion Environment. *J. Coast. Res.* **2020**, *111*, 56–62. [CrossRef]
47. Ren, D.; Yan, C.; Duan, P.; Zhang, Z.; Li, L.; Yan, Z. Durability performances of wollastonite, tremolite and basalt fiber-reinforced metakaolin geopolymer composites under sulfate and chloride attack. *Constr. Build. Mater.* **2017**, *134*, 56–66. [CrossRef]

48. Fan, X.C.; Wu, D.; Chen, H. Experimental Research on the Freeze-Thaw Resistance of Basalt Fiber Reinforced Concrete. *Adv. Mater. Res.* **2014**, *3149*, 1912–1915. [CrossRef]
49. Sim, J.; Park, C.; Moon, D.Y. Characteristics of basalt fiber as a strengthening material for concrete structures. *Compos. Part B Eng.* **2005**, *36*, 504–512. [CrossRef]
50. Ludovico, M.D.; Prota, A.; Manfredi, G. Structural Upgrade Using Basalt Fibers for Concrete Confinement. *J. Compos. Constr.* **2010**, *14*, 541–552. [CrossRef]
51. *GB175–2007*; Standard for Common Portland Cement. Chinese Standard: Beijing, China, 2007. (In Chinese)
52. *GB/T51003/2014*; Technical Code for Application of Mineral Admixture. Chinese Standard: Beijing, China, 2014. (In Chinese)
53. Ipek, M.; Yilmaz, K.; Suemer, M.; Saribiyik, M. Effect of pre-setting pressure applied to mechanical behaviours of reactive powder concrete during setting phase. *Constr. Build. Mater.* **2011**, *25*, 61–68. [CrossRef]
54. Xu, J.; Wang, J.; Zheng, C. Study on reinforcement mechanism and microscopic morphology of steel-basalt mixed fiber HPCC. *Constr. Build. Mater.* **2020**, *256*, 119480. [CrossRef]
55. Wenjun, L.; Hanbing, L.; Bing, Z.; Xiang, L.; Xin, G.; Chunyu, L. Mechanical Properties and Freeze–Thaw Durability of Basalt Fiber Reactive Powder Concrete. *Appl. Sci.* **2020**, *10*, 5682.
56. Hanbing, L.; Shiqi, L.; Peilei, Z.; Yuwei, Z.; Yubo, J. Mechanical Properties and Crack Classification of Basalt Fiber RPC Based on Acoustic Emission Parameters. *Appl. Sci.* **2019**, *9*, 3931.
57. *GB/T 50080–2016*; Standard for Test Method of Performance on Ordinary Fresh Concrete. Ministry of Housing and Urban-Rural Development of the People's Republic of China: Beijing, China, 2016. (In Chinese)
58. *JG/T 248–2009*; Apparatus for Concrete Slump Test. Ministry of Housing and Urban-Rural Development of the People's Republic of China: Beijing, China, 2009. (In Chinese)
59. *GB/T31387–2015*; Reactive Powder Concrete. General Administration of Quality Supervision, Inspection and Quarantine of the People's Republic of China: Beijing, China, 2015. (In Chinese)
60. Yu, R.; Zhou, F.; Yin, T.; Wang, Z.; Ding, M.; Liu, Z.; Leng, Y.; Gao, X.; Shui, Z. Uncovering the approach to develop ultra-high performance concrete (UHPC) with dense meso-structure based on rheological point of view: Experiments and modeling. *Constr. Build. Mater.* **2020**, *271*, 121500. [CrossRef]
61. Nadeem, A.; Memon, S.A.; Lo, T.Y. The performance of Fly ash and Metakaolin concrete at elevated temperatures. *Constr. Build. Mater.* **2014**, *62*, 67–76. [CrossRef]
62. Yuan, H.; Ge, Z.; Sun, R.; Xu, X.; Lu, Y.; Ling, Y.; Zhang, H. Drying shrinkage, durability and microstructure of foamed concrete containing high volume lime mud-fly ash. *Constr. Build. Mater.* **2022**, *327*, 126990. [CrossRef]
63. Elshazli, M.T.; Ramirez, K.; Ibrahim, A.; Badran, M. Mechanical, Durability and Corrosion Properties of Basalt Fiber Concrete. *Fibers* **2022**, *10*, 10. [CrossRef]
64. Ramesh, B.; Eswari, S. Mechanical behaviour of basalt fibre reinforced concrete: An experimental study. *Mater. Today Proc.* **2021**, *43*, 2317–2322. [CrossRef]
65. Zhang, C.; Wang, Y.; Zhang, X.; Ding, Y.; Xu, P. Mechanical properties and microstructure of basalt fiber-reinforced recycled concrete. *J. Clean. Prod.* **2021**, *278*, 123252. [CrossRef]
66. Wang, D.H.; Han, L.; Ju, Y.Z.; Bai, J.F.; Fan, Y.T. Experimental Study on Tensile Properties of Basalt Fiber Reactive Powder Concrete. *Strength Mater.* **2021**, *53*, 670–674. [CrossRef]
67. Haiyang, S.; Jinchun, L. Static mechanical properties of reactive powder concrete reinforced with basalt fibers. *Struct. Concr.* **2022**, *23*, 1675–1686.
68. Zhang, Y.; Liu, J.; Wang, J.; Wu, B. Effect of Hybrid Steel-Basalt Fiber on Behaviors of Manufactured Sand RPC and Fiber Content Optimization Using Center Composite Design. *Adv. Civ. Eng.* **2020**, *2020*, 8877750. [CrossRef]
69. Wang, L.; Zhou, S.; Shi, Y.; Huang, Y.; Zhao, F.; Huo, T.; Tang, S. The Influence of Fly Ash Dosages on the Permeability, Pore Structure and Fractal Features of Face Slab Concrete. *Fractal Fract.* **2022**, *6*, 476. [CrossRef]
70. Peng, Y.; Tang, S.; Huang, J.; Tang, C.; Wang, L.; Liu, Y. Fractal analysis on pore structure and modeling of hydration of magnesium phosphate cement paste. *Fractal Fract.* **2022**, *6*, 337. [CrossRef]
71. Liu, S.F.; Dang, Y.G.; Fang, Z.G.; Xie, N.M. *The Grey System Theory and Its Applications*; Chinese Science Publishing Press: Beijing, China, 2010. (In Chinese)
72. Lza, B.; Cheng, Z.B.; Jd, B. Prediction of compressive strength of recycled aggregate concrete based on gray correlation analysis. *Constr. Build. Mater.* **2021**, *273*, 121750.
73. Wang, X.; Yang, W.; Ge, Y.; Decheng, F. The influence of shrinkage-reducing agent solution properties on shrinkage of cementitious composite using grey correlation analysis. *Constr. Build. Mater.* **2020**, *264*, 120194.
74. Gao, D.; Zhang, L.; Nokken, M. Compressive behavior of steel fiber reinforced recycled coarse aggregate concrete designed with equivalent cubic compressive strength. *Constr. Build. Mater.* **2017**, *141*, 235–244. [CrossRef]
75. Kazmi, S.M.S.; Munir, M.J.; Wu, Y.-F.; Patnaikuni, I. Effect of macro-synthetic fibers on the fracture energy and mechanical behavior of recycled aggregate concrete. *Constr. Build. Mater.* **2018**, *189*, 857–868. [CrossRef]
76. Dong, C.H.; Ma, X.W. Experimental Research on Mechanical Properties of Basalt Fiber Reinforced Reactive Powder Concrete. *Adv. Mater. Res.* **2014**, *893*, 610–613. [CrossRef]
77. Shen, T.; Dong, C.; Wang, H.; Ma, X. Effects of basalt fibers on the electrical flux and mechanical properties of RPC. *Low Temp. Build. Technol.* **2014**, *36*, 1–2. (In Chinese)